

# Pairwise Distance-Diffusion Analysis (PDDA): A Geometric Framework for Estimating Hurst Exponents in Multivariate Long-Memory Processes

Diogo C. Soriano,<sup>1</sup> Frederique Vanheusden,<sup>2</sup> and Slawomir J. Nasuto<sup>3</sup>

<sup>1</sup>*Federal University of ABC, São Bernado do Campo, Brazil.*

<sup>2</sup>*Nottingham Trent University, Nottingham, United Kingdom.*

<sup>3</sup>*University of Reading, Reading, United Kingdom*

(Dated: May 22, 2026)

We introduce Pairwise Distance–Diffusion Analysis (PDDA), a geometric framework for estimating the Hurst exponent from distance plots of long-memory stochastic processes. A single construction yields two complementary routes: R/S–PDDA, a geometric reformulation of the classical rescaled–range definition, and MSD–PDDA, based on mean-squared-displacement scaling, classically used in anomalous diffusion. We extend PDDA to multivariate isotropic and anisotropic processes and derive an explicit link between temporal persistence, range dimension, and recurrence statistics, providing a unified distance-based foundation for Hurst analysis.

## INTRODUCTION

Long-range temporal dependence and anomalous diffusion are central features of complex systems across physics, biology, neuroscience, and economics. In biological and critical systems, long-range correlations are often discussed in terms of scale invariance and  $1/f$  noise [1, 2], whereas in finance and econophysics related phenomena are framed through fractal market hypotheses and persistent volatility [3]. In parallel, anomalous diffusion theory focuses on single-particle dynamics, characterizing deviations of mean-squared displacement from classical Brownian scaling [4, 5]. Despite differences in language and methodology, these perspectives share a common quantitative descriptor: the Hurst exponent  $H$ , which governs both long-memory effects and non-Brownian diffusive scaling [6–9].

Here we introduce *Pairwise Distance–Diffusion Analysis* (PDDA), a geometric framework for estimating the Hurst exponent directly from pairwise distances between cumulative states of a stochastic process. PDDA yields two complementary estimators derived from distance plots. The first, termed R/S-PDDA, recasts the classical rescaled–range definition of  $H$  in geometric terms, expressing persistence through the growth of distance extrema. The second, MSD-PDDA, estimates  $H$  from the scaling of time-averaged mean-squared displacement extracted from diagonal distance profiles, thereby connecting distance plots to variance-scaling laws central to anomalous diffusion theory [4, 10]. This construction builds on the exact correspondence between distance plots and second-order statistics established by Rohde *et al.* [11], which we extend here to scaling regimes characteristic of long-memory processes.

Beyond unifying these two estimation routes, PDDA naturally generalizes to multivariate stochastic processes. Under isotropic conditions, both estimators recover the common persistence exponent, whereas under anisotropy they exhibit distinct mechanisms: R/S-PDDA asymptotically tracks the most persistent direction through geometric diameters, while MSD-PDDA yields a scale-dependent effective exponent reflecting mixed power-law contributions. These behaviors are systematically characterized using Monte Carlo simulations of fractional Brownian motion and fractional Gaussian noise modeled via ARFIMA (Autoregressive Fractionally Integrated Moving Average) processes, within regimes where ergodicity and scaling are well defined [7, 9].

Finally, drawing on the theory of the range dimension of fractional Brownian motion [12–14], we derive an explicit relation linking temporal persistence to spatial occupancy. This result couples the Hurst exponent to the range dimension of the cumulative trajectory, establishing a direct bridge between distance-based scaling, recurrence statistics [15], and fractal geometry. By formulating long-memory analysis in a unified geometric language, PDDA provides a robust and extensible framework for studying persistence in high-dimensional and multivariate systems.

## THEORETICAL BACKGROUND

### Reinterpreting the Hurst exponent from distance plots

The Hurst exponent, classically defined through rescaled–range (R/S) analysis, quantifies how fluctuations of a cumulative process scale with observation length [3, 9]. Here we recast this scaling in geometric terms, expressing  $H$

directly through pairwise distances between cumulative states and extending the formulation to higher-dimensional settings.

**Route 1 (R/S-PDDA): Recasting R/S scaling via distance plots.** Let  $\{X_t\}_{t=1}^N$  be a zero-mean stationary process and  $Z_t$  the cumulative deviate path given its intergrated form:

$$Z_t = \sum_{i=1}^t (X_i - \bar{X}), \quad t = 1, \dots, N. \quad (1)$$

The Hurst exponent  $H$  quantifies how the amplitude of its fluctuations grows with the time scale [3, 9]. In the classical (R/S) analysis, the range and standard deviation over a window of length  $n$  are defined as:

$$R(n) = \max_{1 \leq t \leq n} Z_t - \min_{1 \leq t \leq n} Z_t, \quad S(n) = \sqrt{\frac{1}{n} \sum_{t=1}^n (X_t - \bar{X})^2}, \quad (2)$$

and the expected ratio scales as:

$$E \left[ \frac{R(n)}{S(n)} \right] \propto n^H. \quad (3)$$

For  $H = 0.5$ , increments are uncorrelated (white noise, or Brownian motion);  $H > 0.5$  corresponds to persistent (or superdiffusion) behavior, while  $H < 0.5$  outlines anti-persistent (or subdiffusion) regimes [3–5, 9]. A distance-based formulation follows directly by defining the distance matrix of the cumulative trajectory [15]:

$$D_{ij} = |Z_i - Z_j|, \quad i, j = 1, \dots, N, \quad (4)$$

and the cumulative-path diameter within a window of length  $n$  can be obtained:

$$R_D(n) = \sqrt{\max_{i,j \leq n} (Z_i - Z_j)^2} = \max_{i,j \leq n} D_{ij}. \quad (5)$$

If we consider  $S_D(n)$  the standard deviation of the increments, this leads exactly to the classical R/S definition in the univariate scenario:

$$E \left[ \frac{R_D(n)}{S_D(n)} \right] \propto n^H. \quad (6)$$

This formulation highlights that  $H$  controls how the geometry of pairwise distances expands with observation length, recasting the Hurst exponent as a measure of the cumulative path's geometric extent in distance-plot space. A purely geometric estimator can then be constructed directly from  $D_{ij}$ .

**Route 2 (MSD-PDDA): Obtaining  $H$  from the distance profile and variance-scaling law.**

The distance profile,

$$M_2(\tau) \equiv \langle D^2(\tau) \rangle = \frac{1}{N - \tau} \sum_{t=1}^{N-\tau} (Z_{t+\tau} - Z_t)^2, \quad (7)$$

defines the mean-squared displacement between cumulative states at lag  $\tau$ . As shown by Rohde *et al.* [11], it is exactly related to second-order statistics:

$$M_2(\tau) = 2[\sigma_Z^2 - C_Z(\tau)], \quad (8)$$

in which  $\sigma_Z^2$  is the variance and  $C_Z(\tau)$  the autocovariance function of  $Z_t$ .

Although this correspondence was established at the level of moments, its scaling implications for long-memory processes were not explored. Here we connect  $M_2(\tau)$  to the power-law variance growth underlying anomalous diffusion and fractional Brownian motion. Indeed, it is well-known that for long-memory increments - such as fractional Gaussian noise or ARFIMA processes - the autocovariance of  $X_t$  decays as [9]:

$$C_X(\tau) \sim \tau^{2H-2}, \quad \tau \rightarrow \infty, \quad (9)$$

For such processes, the variance of the cumulative sum (the deviation process  $Z_t$ ) obeys [7, 9, 16]:

$$\mathbb{E}[(Z_{t+\tau} - Z_t)^2] \sim \tau^{2H}, \quad \tau \rightarrow \infty, \quad (10)$$

The distance profile  $M_2(\tau)$  defines as an empirical estimator of  $\mathbb{E}[(Z_{t+\tau} - Z_t)^2]$  and directly approximates the variance term in Eq. (10), while inheriting its scaling law:

$$M_2(\tau) \asymp \tau^{2H}, \quad \tau \rightarrow \infty. \quad (11)$$

Taking logarithms from both sides and isolating  $H$ :

$$H = \frac{1}{2} \frac{d(\log M_2(\tau))}{d(\log \tau)}. \quad (12)$$

The slope of  $\log M_2(\tau)$  versus  $\log \tau$  therefore *provides a purely geometric estimator of the Hurst exponent*, derived directly from the distance plot without reference to ranges or standard deviations.

**Contribution 1 — Unified interpretation.** Equations (6) and (12) define the Hurst exponent as a geometric scaling of pairwise distances: via range–dispersion growth (R/S-PDDA), commonly used in the long-range dependence literature, and via mean-squared-displacement scaling (MSD-PDDA), in anomalous diffusion. While these formulations are traditionally treated separately, PDDA shows they are complementary projections of the same trajectory expansion law and formulates both explicitly in the distance–plot domain.

By operating in the distance–plot domain, this framework favors the generalization to multivariate systems, where pairwise distances replace the unidimensional notion of range, allowing the Hurst exponent to be defined in a coordinate–invariant geometric form.

### Generalizing PDDA for multivariate long-memory processes

Let  $\mathbf{X}_t \in \mathbb{R}^m$  denote an  $m$ -variate long-memory process, as given by an  $m$ -variate ARFIMA(0,  $\mathbf{d}$ , 0) written as [17, 18]:

$$\mathbf{X}_t = \sum_{k \geq 0} a_k \boldsymbol{\varepsilon}_{t-k}, \quad \boldsymbol{\varepsilon}_t \sim \mathcal{N}(\mathbf{0}, \Sigma_\rho), \quad (13)$$

where the fractional integration coefficients satisfy:

$$a_0 = 1, \quad a_k = a_{k-1} \frac{k-1+d}{k}, \quad (14)$$

and the innovation covariance:

$$\Sigma_\rho = \begin{pmatrix} 1 & \rho \\ \rho & 1 \end{pmatrix}, \quad (15)$$

controls the instantaneous cross-correlation between coordinates. Here,  $d = H - 0.5$  represents the fractional integration parameter. Each marginal coordinate may exhibit its own Hurst exponent:

$$X_t^{(k)} \sim \text{fGn}(H_k), \quad k = 1, \dots, m.$$

The multidimensional cumulative trajectory is defined as:

$$\mathbf{Z}_t = \sum_{i=1}^t (\mathbf{X}_i - \bar{\mathbf{X}}), \quad (16)$$

generalizing Eq. (1), with the corresponding distance matrix:

$$D_{ij} = \|\mathbf{Z}_i - \mathbf{Z}_j\|, \quad (17)$$

in which  $\|\cdot\|$  denotes the Euclidean norm.

**Route 1 (R/S-PDDA): DP-based rescaled-range geometry in  $\mathbb{R}^m$**

For a block of size  $n$ , define the multivariate diameter and dispersion:

$$R_D(n) = \max_{i,j \leq n} \|\mathbf{Z}_i - \mathbf{Z}_j\|, \quad S_D(n) = \sqrt{\text{tr Cov}(\mathbf{X}_1, \dots, \mathbf{X}_n)}, \quad (18)$$

in which  $\text{tr Cov}(\cdot)$  is the trace of the covariance matrix and  $S_D(n)$  represents a generalized measure of data spread in the  $m$ -dimensional space. This allows to obtain the analogue of the classical R/S law in the form:

$$\mathbb{E} \left[ \frac{R_D(n)}{S_D(n)} \right] \propto n^{H_{\text{multi}}}. \quad (19)$$

*Isotropic case.* If all coordinates share the same Hurst exponent  $H_1 = \dots = H_m = H$ , then  $H_{\text{multi}} = H$ . The geometry of  $\mathbf{Z}_t$  is simply a rotated and scaled version of the univariate trajectory, given that the instantaneous cross-correlation between coordinates only modifies prefactors, not the slope in  $\ln(R_D/S_D)$  (see Supplementary Material S1.2 and S3.2).

*Anisotropic case.* When  $H_1, \dots, H_m$  differ, the diameter in (19) is governed by the most persistent coordinate:

$$R_D(n) \asymp n^{H_{\text{max}}}, \quad H_{\text{max}} := \max_k H_k. \quad (20)$$

Thus,

$$H_{\text{multi}} = H_{\text{max}}. \quad (21)$$

R/S-PDDA therefore acts as a max-selector, converging to the largest persistence exponent, since the Euclidean diameter is dominated by the direction of maximal long-range excursions.

**Route 2 (MSD-PDDA): Variance scaling via the distance profile**

The distance-profile estimator extends naturally to the vector case:

$$M_2(\tau) = \langle \|\mathbf{Z}_{t+\tau} - \mathbf{Z}_t\|^2 \rangle. \quad (22)$$

Using  $\Delta_\tau \mathbf{Z}_t = \mathbf{Z}_{t+\tau} - \mathbf{Z}_t$ , we expand:

$$M_2(\tau) = \sum_{k=1}^m \mathbb{E} \left[ (\Delta_\tau Z_t^{(k)})^2 \right], \quad (23)$$

in which each coordinate contribute with a term proportional to  $\tau^{2H_k}$ :

$$M_2(\tau) \approx c_1 \tau^{2H_1} + c_2 \tau^{2H_2} + \dots + c_m \tau^{2H_m}, \quad c_k > 0. \quad (24)$$

*Isotropic case.* If  $H_k \equiv H$ , then:

$$M_2(\tau) \propto \tau^{2H}, \quad H_{\text{multi}} = H. \quad (25)$$

*Anisotropic case.* Equation (24) shows that  $M_2(\tau)$  is a *mixture of power laws*. Its slope in log-log coordinates:

$$H_{\text{eff}}(\tau) = \frac{1}{2} \frac{d(\ln M_2(\tau))}{d(\ln \tau)}, \quad (26)$$

is scale-dependent:

$$H_{\text{eff}}(\tau) \approx \begin{cases} \text{close to a weighted average of } \{H_k\}, & \tau \rightarrow 1, \\ H_{\text{max}}, & \tau \rightarrow \infty, \end{cases} \quad (27)$$

a result derived formally in the S1.1. Thus, *small lags* emphasize a combination of directions' persistency, while *large lags* tends to track the most persistent exponent  $H_{\text{max}}$ .

Accordingly, the global MSD-PDDA estimate obtained from a large-lag regression window converges to  $H_{\text{max}}$ , matching R/S-PDDA asymptotically while offering improved finite-sample behavior due to averaging across all increment pairs.

**Contribution 2 — Multivariate generalization.** We introduce a geometric formulation of the multivariate Hurst exponent, in which persistence is inferred from pairwise distances. This framework reveals that effective multivariate scaling obeys distinct mechanisms: R/S-PDDA selects the dominant persistence direction, whereas MSD-PDDA captures scale-dependent mixtures of exponents. They ( $\tau$ ) converge asymptotically.

These scaling relations identify the Hurst exponent as a geometric property of the cumulative trajectory encoded by pairwise distances. To understand the broader significance of this geometry, it is useful to interpret the distance–plot representation within the framework of fractal measures in state space.

### Fractal dimension of the range and its relation to the Hurst exponent

A central object underlying distance and recurrence analysis is the *range* of a stochastic process, defined as the set of values visited by its cumulative trajectory in state space [13],

$$\mathcal{R} = \{\mathbf{Z}(t) : t \in \mathbb{R}\} \subset \mathbb{R}^m. \quad (28)$$

For self-similar long-memory processes such as fractional Brownian motion (fBm), fractional Gaussian noise (fGn), and ARFIMA models, the geometry of  $\mathcal{R}$  is not arbitrary: it exhibits fractal structure governed by the Hurst exponent  $H$ . In particular, the *range dimension*

$$D_{\text{range}} = \min\{m, 1/H\}, \quad (29)$$

quantifies how the trajectory fills the embedding space  $\mathbb{R}^m$ . This concept was originally introduced by Mandelbrot [12] and later established rigorously in [13, 14]. Rough processes ( $H$  small) rapidly explore all spatial directions and yield  $D_{\text{range}} = m$ , whereas smoother processes ( $H$  large) evolve on a lower-dimensional subset with  $D_{\text{range}} = 1/H$ .

Distance and recurrence plots naturally probe this range geometry because they are constructed from pairwise separations  $\|\mathbf{Z}_i - \mathbf{Z}_j\|$  between states. Varying the distance threshold  $\varepsilon$  at fixed lag therefore measures how the points of  $\mathcal{R}$  populate space, directly accessing  $D_{\text{range}}$  (see S1.3), as also classically performed using correlation integrals for estimating fractal dimension of strange attractors [19].

To connect this spatial geometry to temporal persistence, consider the probability that two states separated by a time lag  $\tau$  remain within a distance  $\varepsilon$ ,

$$P(\varepsilon, \tau) = \Pr(\|\mathbf{Z}_{t+\tau} - \mathbf{Z}_t\| \leq \varepsilon). \quad (30)$$

The typical scale of state-space displacements is given by the root–mean–square increment,

$$\sigma(\tau) = \sqrt{\mathbb{E}[\|\mathbf{Z}_{t+\tau} - \mathbf{Z}_t\|^2]} \propto \tau^H, \quad (31)$$

which characterizes how fluctuations grow with the observation scale.

Normalizing separations by  $\sigma(\tau)$  yields:

$$P(\varepsilon, \tau) = \Pr\left(\left\|\frac{\mathbf{Z}_{t+\tau} - \mathbf{Z}_t}{\sigma(\tau)}\right\| \leq \frac{\varepsilon}{\sigma(\tau)}\right). \quad (32)$$

For a small argument  $x$ ,  $Pr(x)$  scales with the volume of a ball in  $D_{\text{range}}$  dimensions ( $x^{D_{\text{range}}}$ ), leading to:

$$P(\varepsilon, \tau) \propto \underbrace{\varepsilon^{D_{\text{range}}}}_{\text{static geometry } (\tau=0)} \underbrace{\tau^{-HD_{\text{range}}}}_{\text{multiscale temporal persistence}}. \quad (33)$$

Equation (33) shows that the decay of recurrence probability is jointly controlled by how far the process typically moves ( $H$ ) and by how many independent spatial directions it can explore ( $D_{\text{range}}$ ). Two regimes follow directly:

- **Rough or space–filling processes** ( $1/H > m$ ):  $D_{\text{range}} = m$ , and  $P(\varepsilon, \tau) \propto \tau^{-mH}$ , so the decay steepens with embedding dimension.
- **Smooth or range–limited processes** ( $1/H < m$ ):  $D_{\text{range}} = 1/H$ , and  $P(\varepsilon, \tau) \propto \tau^{-1}$ , yielding a universal decay independent of  $H$  and  $m$ .

The quantity  $M_2(\tau)$  introduced earlier captures the same persistence scaling without thresholding, measuring the growth of typical displacements, whereas  $P(\varepsilon, \tau)$  quantifies the probability of remaining close to. Their unified scaling form,

$$P(\varepsilon, \tau) \propto \varepsilon^{D_{\text{range}}} \tau^{-HD_{\text{range}}}, \quad (34)$$

provides a geometric interpretation of long-memory processes in which spatial occupancy and temporal persistence are inseparable.

**Contribution 3 — Bridging Hurst exponent and distance-plot range dimension.** Eq. (34) captures the joint scaling between temporal persistence and spatial occupancy,

$$P(\varepsilon, \tau) \propto \varepsilon^{D_{\text{range}}} \tau^{-HD_{\text{range}}},$$

linking the geometry of the process range ( $D_{\text{range}}$ ) to its temporal memory ( $H$ ). In one dimension the decay exponent reduces to  $-H$ . In higher dimensions, the decay reflects the effective range dimension: for rough (anti-persistent) processes ( $H < 1/m$ ) it scales as  $-mH$ , whereas for smoother (persistent) processes it saturates at the universal limit  $-1$ , independently of  $m$ . Thus, Eq. (34) unifies temporal and spatial scaling through a clear crossover between dimension-controlled and persistence-controlled regimes.

Finally, Eq. (34) establishes a precise connection with recurrence quantification analysis (RQA). In standard RQA, the diagonal-wise recurrence rate  $RR(\tau)$  defines the generalized autocorrelation function  $\hat{p}(\tau)$  [15]. While RQA trend measures quantify linear decay with  $\tau$ , they do not capture the scale-invariant log-log structure characteristic of fractional noise. Equation (34) clarifies that recurrence decay is governed by the combined action of temporal persistence and range geometry, explaining why direct links between RQA metrics and the Hurst exponent remain ambiguous in multivariate and embedded settings unless the role of  $D_{\text{range}}$  is made explicit.

## RESULTS

In the following, the theoretical framework is validated using ARFIMA simulations across a broad range of parameters. Details concerning the simulations can be found in the supplemental material (S2).

*Univariate Scenario - Equivalence.* Figure 1 validates the equivalence between classical R/S analysis and its distance-based counterpart. For ARFIMA processes spanning anti-persistent, Brownian, and persistent regimes ( $H = 0.25, 0.5, 0.75$ ), both R/S-PDDA and MSD-PDDA recover the theoretical scaling in  $M_2(\tau) \sim 2H \ln \tau$ . While both estimators are asymptotically consistent, MSD-PDDA exhibits reduced bias in the anti-persistent regime.

Estimator performance is summarized in Tables I and II. For intermediate sample sizes, R/S-PDDA overestimates  $H$  in the anti-persistent regime ( $H < 0.5$ ), whereas MSD-PDDA achieves lower RMSE; for strongly persistent dynamics ( $H \gtrsim 0.65$ ), R/S-PDDA becomes slightly more accurate. In the asymptotic regime, both estimators converge, with MSD-PDDA retaining lower variance across all  $H$  values.

TABLE I: **Estimator comparison for  $N = 2048$  (intermediate-sample regime).**

$H_T$	R/S-PDDA (Route 1)			MSD-PDDA (Route 2)		
	Bias	SD	RMSE	Bias	SD	RMSE
0.10	0.1699	0.0236	0.1715	0.0532	0.0372	<b>0.0649</b>
0.25	0.1075	0.0284	0.1112	0.0170	0.0393	<b>0.0426</b>
0.35	0.0698	0.0294	0.0757	-0.0022	0.0387	<b>0.0385</b>
0.50	0.0379	0.0351	0.0516	-0.0113	0.0454	<b>0.0465</b>
0.65	0.0107	0.0408	<b>0.0420</b>	-0.0189	0.0458	0.0493
0.75	-0.0044	0.0480	<b>0.0480</b>	-0.0401	0.0478	0.0622
0.90	-0.0601	0.0470	<b>0.0761</b>	-0.0912	0.0460	0.1021

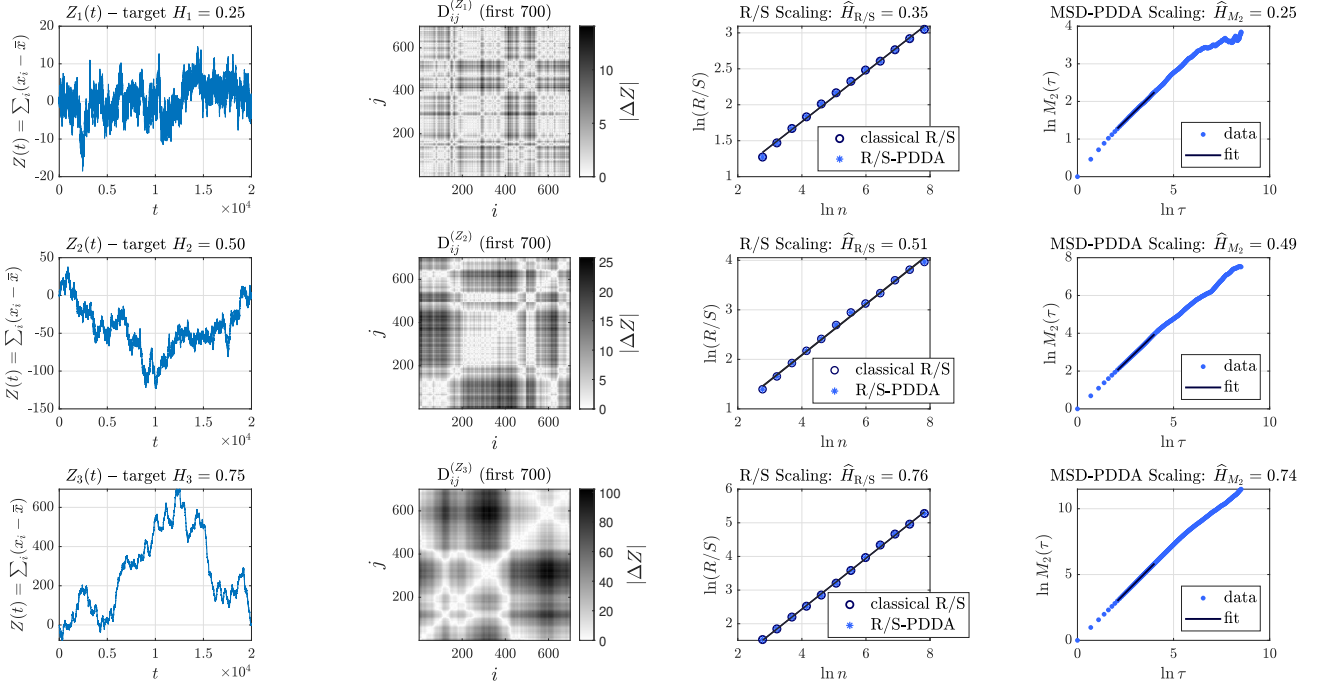


FIG. 1: **Univariate ARFIMA simulations and Hurst estimation via distance plots** ( $N = 2 \times 10^4$ ). Rows correspond to  $H = 0.25, 0.50$ , and  $0.75$ . Left: cumulative paths  $Z(t)$ . Middle-left: distance plots  $D_{ij}^{(Z)}$  showing increasing spatial coherence with  $H$ . Middle-right: R/S-PDDA scaling (classical R/S: open circles; DP-based: blue stars). Right: MSD-PDDA scaling from  $M_2(\tau)$ . Slopes from log-log fits yield  $\hat{H}_{R/S}$  and  $\hat{H}_{M_2}$  (panel titles).

TABLE II: **Estimator comparison for  $N = 32768$  (high-sample regime).**

$H_T$	R/S-PDDA (Route 1)			MSD-PDDA (Route 2)		
	Bias	SD	RMSE	Bias	SD	RMSE
0.10	0.1302	0.0078	0.1304	0.0582	0.0076	<b>0.0587</b>
0.25	0.0733	0.0102	0.0740	0.0188	0.0097	<b>0.0211</b>
0.35	0.0491	0.0122	0.0505	0.0043	0.0103	<b>0.0111</b>
0.50	0.0222	0.0161	0.0274	-0.0009	0.0121	<b>0.0121</b>
0.65	0.0070	0.0170	0.0183	-0.0031	0.0119	<b>0.0122</b>
0.75	-0.0036	0.0200	0.0202	-0.0054	0.0113	<b>0.0125</b>
0.90	-0.0353	0.0228	0.0420	-0.0329	0.0161	<b>0.0366</b>

*Multivariate isotropic and anisotropic processes.* Figures 2 and 3 characterize the behavior of the distance-based estimators under isotropic multivariate dynamics ( $H_1 = H_2$ ). Figure 2 shows that, independently of the dimensionality of the process, distance plots provide an effective two-dimensional representation of the cumulative trajectory, whose texture directly reflects the spatial coherence associated with the Hurst exponent. In this setting, MSD-PDDA consistently yields more accurate estimates in the anti-persistent regime, whereas both routes perform comparably for persistent dynamics at this sample size.

Figure 3 quantifies these trends across  $H_T$ . Both estimators exhibit consistent scaling over the full range of persistence, confirming the robustness of the geometric formulation. MSD-PDDA achieves minimal bias and lowest RMSE around  $H_T \approx 0.45$  and remains superior throughout the anti-persistent and weakly persistent regimes, while R/S-PDDA becomes preferable only for strongly persistent processes ( $H_T \gtrsim 0.65$ ). These results show that both estimators probe complementary aspects of persistence: MSD-PDDA provides a statistically efficient route for low-sample and anti-persistent dynamics, whereas R/S-PDDA becomes competitive as long-range coherence dominates.

In the anisotropic setting, we simulate ARFIMA processes with fixed  $H_2 = 0.30$  and  $\rho = 0.3$ , and sweep  $H_1 \in [0.10, 0.90]$ .  $H_{\max} = \max\{H_1, H_2\}$  was considered as the reference exponent. Figure 4(a) shows that R/S-PDDA tracks

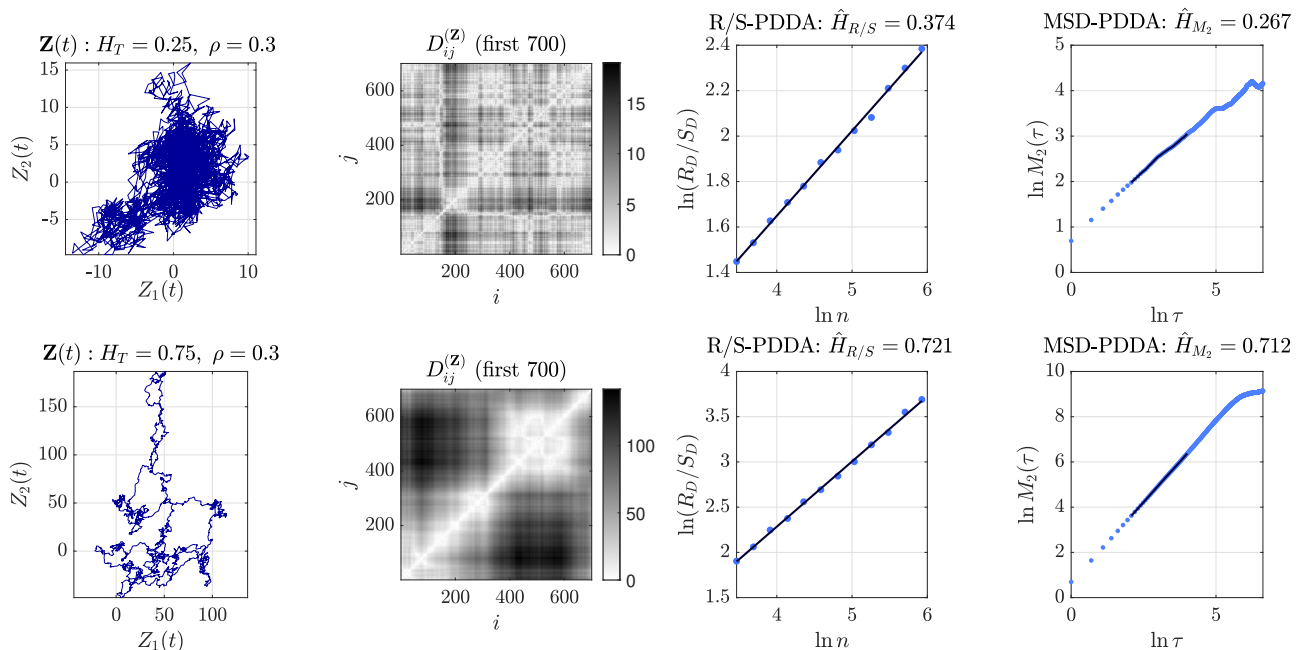


FIG. 2: **Bivariate isotropic ARFIMA: anti- vs persistent regimes** ( $N = 3000$ ,  $\rho = 0.3$ ). Rows correspond to  $H_1 = H_2 = 0.25$  (top) and  $H_1 = H_2 = 0.75$  (bottom). Columns show: cumulative path  $\mathbf{Z}$ ; distance plot  $D_{ij}^{(\mathbf{Z})}$  (first 700 samples); R/S-PDDA scaling,  $\ln(R_D/S_D)$  vs.  $\ln n$ ; and MSD-PDDA scaling,  $\ln M_2(\tau)$  vs.  $\ln \tau$ . MSD-PDDA better approximates  $H$  in the anti-persistent regime, while both estimators perform comparably for persistent dynamics. Estimated slopes are reported in panel titles.

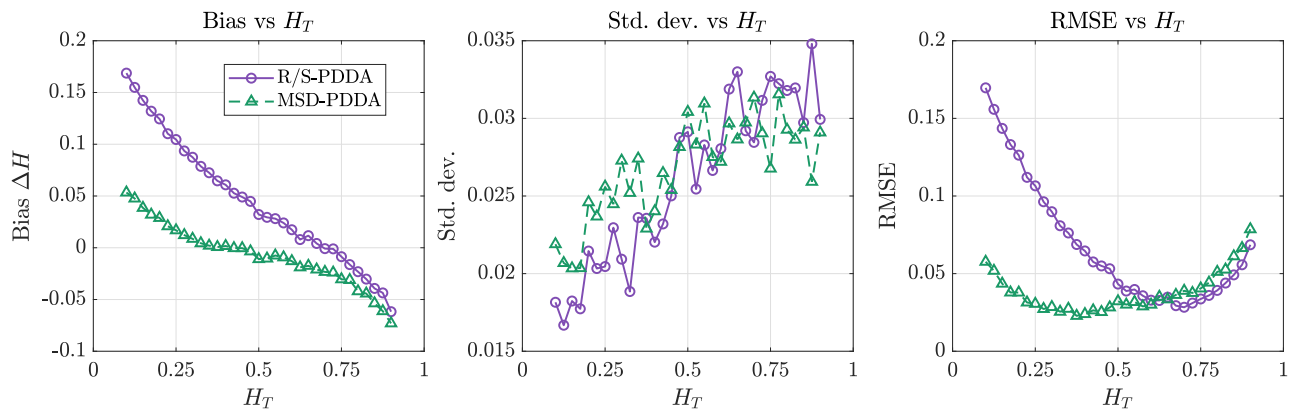


FIG. 3: **Estimator behavior across Hurst regimes in bivariate isotropic ARFIMA**. Results for  $\rho = 0.3$ ,  $N = 3000$ , and  $R = 100$ . Panels show bias (left), standard deviation (center), and RMSE (right) of  $\hat{H}_{R/S}$  (purple) and  $\hat{H}_{M_2}$  (green) versus  $H_T$ . MSD-PDDA yields lower bias and RMSE in the anti-persistent regime ( $H_T < 0.5$ ), while R/S-PDDA becomes slightly more accurate for strongly persistent dynamics ( $H_T \gtrsim 0.65$ ). Minimal error occurs near  $H_T \approx 0.45$ .

$H_{\max}$  once  $H_1 > H_2$ , but overestimates persistence in the strongly anti-persistent regime ( $H_1 < H_2$ ), consistent with diameter-based dominance by the most persistent direction. MSD-PDDA follows the overall trend but systematically underestimates  $H_{\max}$ .

Figure 4(b) explains this behavior for a representative case  $(H_1, H_2) = (0.25, 0.50)$ . The local slope  $H_{\text{loc}}(\tau)$  transitions from the mean  $(H_1 + H_2)/2$  at small lags to the dominant exponent at larger  $\tau$ , consistent with Eq. (26). As MSD-PDDA relies on an intermediate fitting window, the resulting estimate lies between the mean and  $H_{\max}$ , accounting for the controlled underestimation observed in panel (a).

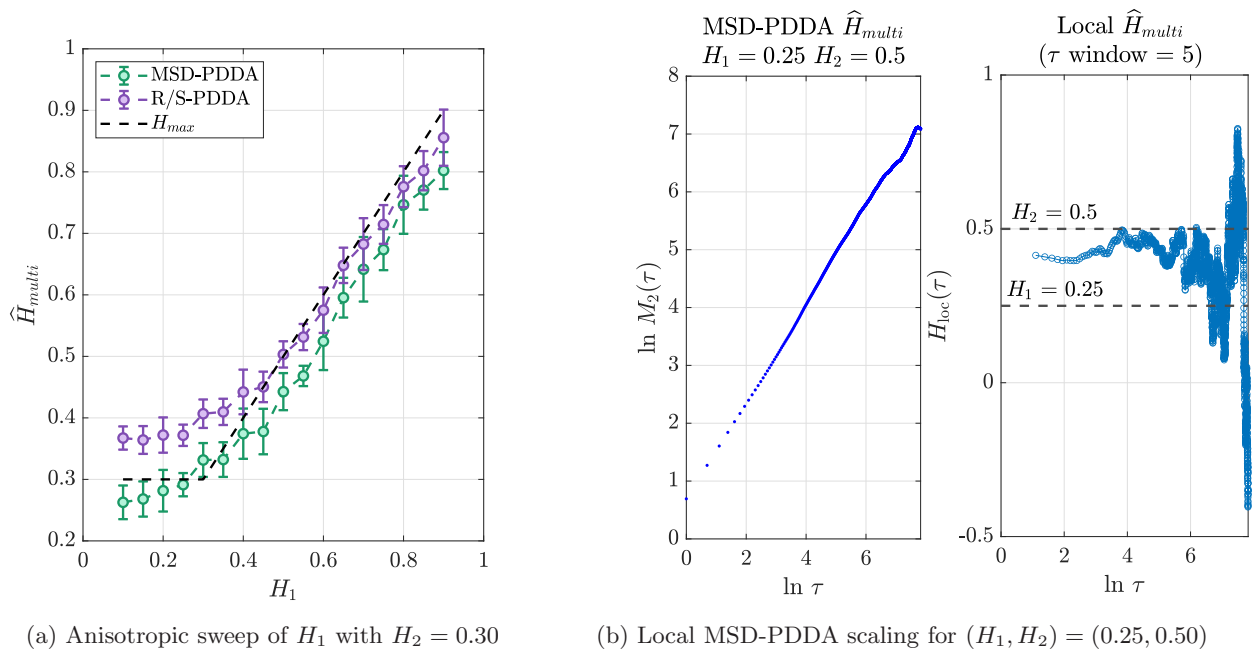


FIG. 4: **Bivariate anisotropic ARFIMA: R/S- vs MSD-PDDA.** (a) Estimated multivariate exponent  $\hat{H}_{\text{multi}}$  versus  $H_1$  for fixed  $H_2 = 0.30$  and  $\rho = 0.3$  ( $N = 3000$ ,  $R = 10$ ). Symbols show mean  $\hat{H}_{\text{multi}}$  with  $\pm 1$  SD; dashed line denotes  $H_{\text{max}} = \max\{H_1, H_2\}$ . R/S-PDDA tracks  $H_{\text{max}}$  in the persistent regime, while MSD-PDDA underestimates but follows the trend. (b) MSD-PDDA scaling for  $(H_1, H_2) = (0.25, 0.50)$ :  $\ln M_2(\tau)$  vs.  $\ln \tau$  (left) and local slope  $H_{\text{loc}}(\tau)$  (right), showing the transition from mixed to dominant scaling.

*Joint geometric–temporal scaling.* Figure 5 tests the scaling law  $P(\varepsilon, \tau) \propto \varepsilon^{D_{\text{range}}} \tau^{-HD_{\text{range}}}$  by fixing  $D_{\text{range}}$  to its theoretical value  $D_{\text{range}}^{\text{th}} = \min\{m, 1/H_{\text{max}}\}$ . The recurrence probability  $P(\varepsilon, \tau)$  was evaluated using a fixed threshold  $\varepsilon = 0.2$  after normalizing each coordinate to unit variance. Despite this non-asymptotically small threshold, the  $\tau$ -dependence exhibits the predicted power-law decay for both isotropic and anisotropic regimes. The agreement between fitted and theoretical slopes confirms that recurrence decay captures a global coupling between temporal persistence and spatial occupancy encoded by the range dimension.

## DISCUSSION

PDDA provides a geometric foundation for Hurst exponent estimation by expressing temporal persistence in terms of distance scaling of cumulative trajectories. A single distance-based construction yields two complementary estimators: a geometric reinterpretation of classical R/S analysis and a variance-based route rooted in anomalous diffusion theory. Their asymptotic equivalence and distinct finite-sample behavior clarify long-standing differences between range- and MSD-based approaches.

In multivariate systems, PDDA reveals how persistence manifests geometrically. R/S-PDDA acts as a max-selector, converging to the most persistent direction, while MSD-PDDA captures scale-dependent mixtures of persistence exponents. Beyond estimation, the derived relation between recurrence probability, range dimension, and Hurst exponent establishes a direct link between temporal memory and spatial occupancy.

From a broader perspective, Eq. (34) can be viewed in light of the correlation integral introduced by Grassberger [19]. Here, the recurrence probability  $P(\varepsilon, \tau)$  plays the role of a lag-specific correlation integral, probing the density of the process range at a given temporal scale  $\tau$ . In contrast to the static geometric characterization of attractors, PDDA effectively “animates” this correlation measure under the scaling laws of anomalous diffusion and long-memory processes. The central contribution is therefore structural: PDDA unifies concepts from long-range dependence, anomalous diffusion, and recurrence analysis under a single geometric object (the distance plot) while naturally extending to multivariate settings. Within this framework, the Hurst exponent is shown to govern generalized correlation decay in high-dimensional spaces through its coupling to the range dimension, providing a precise

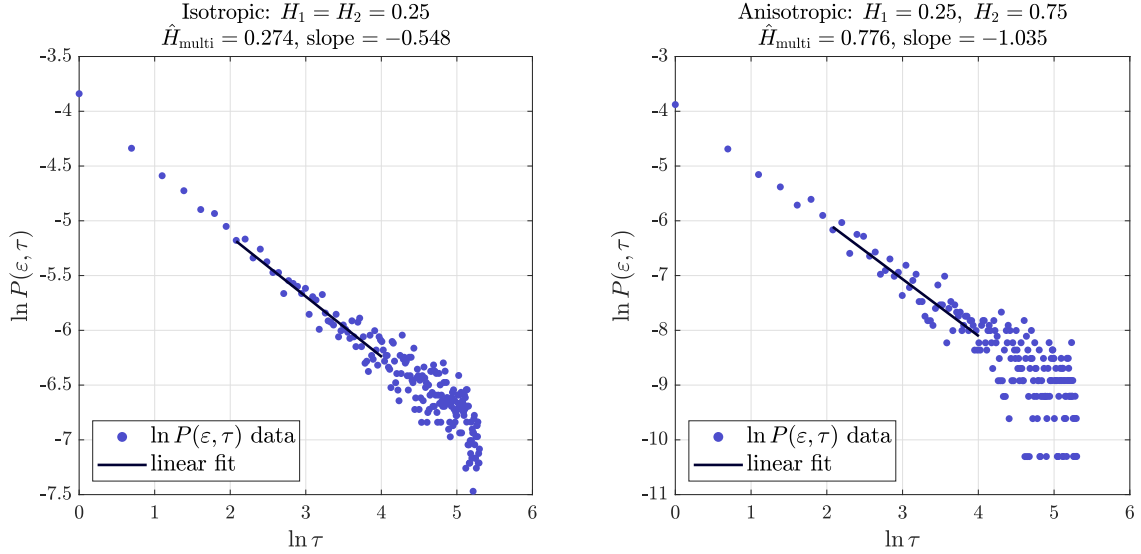


FIG. 5: Numerical test of the range–dimension scaling law in Eq. (34). Shown is  $\ln P(\varepsilon, \tau)$  versus  $\ln \tau$  (dots) with linear fits over  $\tau \in [8, 55]$  (solid lines) for bivariate ARFIMA processes ( $N = 30000$ ,  $m = 2$ ,  $\rho = 0.3$ ). *Left*: isotropic case  $H_1 = H_2 = 0.25$ , for which  $D_{\text{range}}^{\text{th}} = 2$  and Eq. (34) predicts a slope  $\approx -0.5$ , in agreement with the fit ( $\approx -0.55$ ). *Right*: anisotropic case  $H_1 = 0.25, H_2 = 0.75$ , yielding  $D_{\text{range}}^{\text{th}} \approx 4/3$  and a predicted unit decay exponent, consistent with the fitted slope ( $\approx -1.04$ ). These results confirm that the decay of  $P(\varepsilon, \tau)$  is governed by the coupled action of temporal persistence and range dimension.

relation between persistence, recurrence probability, and spatial geometry.

#### ACKNOWLEDGMENTS

DCS acknowledges support from CNPq (31397/2023-8) and FAPESP (2019/09512-0).

#### DATA AVAILABILITY

All codes for generating figures and use PDDA can be found in: <https://github.com/dcsoriano/GitHub---PDDA>

- 
- [1] P. Bak, C. Tang, and K. Wiesenfeld, *Physical Review Letters* **59**, 381 (1987).
  - [2] M. S. A. Ferraz, A. R. Muotri, and A. H. Kihara, *Physical Review Letters* **135**, 108402 (2025).
  - [3] E. E. Peters, *Fractal Market Analysis: Applying Chaos Theory to Investment and Economics*, Wiley Finance Editions (John Wiley & Sons, New York, 1994).
  - [4] R. Metzler, J.-H. Jeon, A. G. Cherstvy, and E. Barkai, *Physical Chemistry Chemical Physics* **16**, 24128 (2014).
  - [5] M. S. Gomes-Filho, L. C. Lapas, E. Gudowska-Nowak, and F. A. Oliveira, *Physics Reports* **1141**, 1 (2025).
  - [6] B. B. Mandelbrot and J. W. Van Ness, *SIAM Review* **10**, 422 (1968), stable URL: <https://www.jstor.org/stable/2027184>.
  - [7] J. Beran, *Statistics for Long-Memory Processes*, Monographs on Statistics and Applied Probability, Vol. 61 (Chapman and Hall, New York, 1994).
  - [8] G. Samorodnitsky and M. S. Taqqu, *Stable Non-Gaussian Random Processes: Stochastic Models with Infinite Variance* (Chapman and Hall, New York, 1994).
  - [9] J. Gao, Y. Cao, W.-w. Tung, and J. Hu, *Multiscale Analysis of Complex Time Series: Integration of Chaos and Random Fractal Theory* (John Wiley & Sons, Hoboken, NJ, 2007).
  - [10] G. Sikora, K. Burnecki, and A. Wyłomańska, *Physical Review E* **95**, 032110 (2017).
  - [11] G. K. Rohde, J. M. Nichols, B. M. Dissinger, and F. Bucholtz, *Physica D: Nonlinear Phenomena* **237**, 619 (2008).
  - [12] B. B. Mandelbrot, *The Fractal Geometry of Nature* (W. H. Freeman and Company, San Francisco, CA, 1982).

- [13] Y. Xiao, in *Fractal Geometry and Applications: A Jubilee of Benoit Mandelbrot*, edited by M. L. Lapidus and M. van Frankenhuijsen (American Mathematical Society, 2004) pp. 261–338.
- [14] D. Wu and Y. Xiao, *Journal of Theoretical Probability* **20**, 203 (2006).
- [15] N. Marwan, M. C. Romano, M. Thiel, and J. Kurths, *Physics Reports* **438**, 237 (2007).
- [16] K. Falconer, *Fractal Geometry: Mathematical Foundations and Applications* (John Wiley & Sons, Chichester, 2003).
- [17] J. R. M. Hosking, *Biometrika* **68**, 165 (1981).
- [18] K. Liu, Y. Chen, and X. Zhang, *Axioms* **6**, 16 (2017).
- [19] P. Grassberger and I. Procaccia, *Physical Review Letters* **50**, 346 (1983).